Article
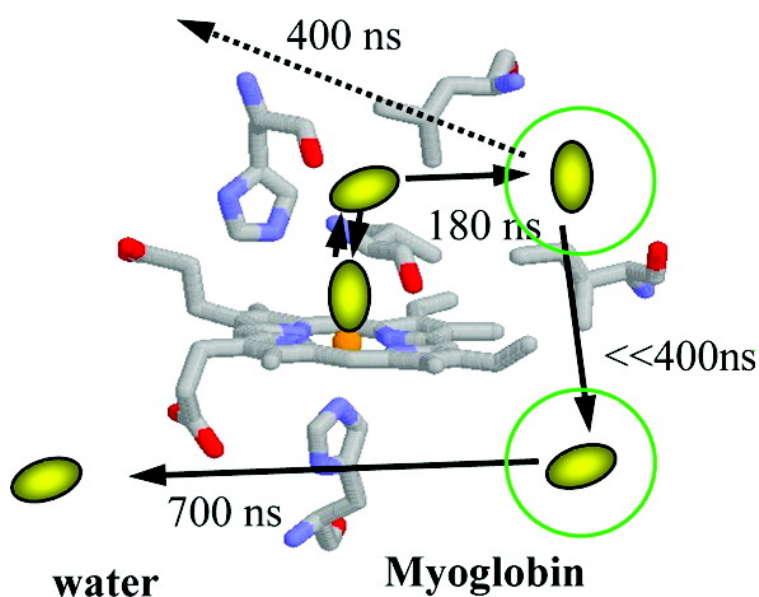
The Escape Process of Carbon Monoxide from Myoglobin to Solution at Physiological Temperature

Yasutaka Nishihara, Masaaki Sakakura, Yoshifumi Kimura, and Masahide Terazima

More About This Article

Additional resources and features associated with this article are available within the HTML version:

- Supporting Information
- Links to the 5 articles that cite this article, as of the time of this article download
- Access to high resolution figures
- Links to articles and content related to this article
- Copyright permission to reproduce figures and/or text from this article

View the Full Text HTML

J|A|C|S
A R T I C L E S

The Escape Process of Carbon Monoxide from Myoglobin to Solution at Physiological Temperature

Yasutaka Nishihara, Masaaki Sakakura, Yoshifumi Kimura, and
Masahide Terazima*

*Contribution from the Department of Chemistry, Graduate School of Science, Kyoto University,
Kyoto, 606-8502, Japan*

Received October 4, 2003; E-mail: mterazima@kuchem.kyoto-u.ac.jp

Abstract: The carbon monoxide (CO) docking sites involved in the ligand escape process from the iron atom in hem of myoglobin (Mb) to solution at physiological temperature were studied on the basis of the effect of xenon (Xe) on the ligand escape rate by the transient grating (TG) technique. The TG method provides a direct measurement of the changes in molecular volume. The apparent CO escaping rate and the volume contraction increase with increasing Xe pressure. The pressure dependence of the rate is consistent with that of the Xe population at the Xe(1) site. This result clearly shows that CO is trapped at the Xe(1) site before escaping to solvent in a Xe-free solution at room temperature. It is shown that only CO but not the trapped Xe is released by the photoexcitation of the Xe-trapped MbCO. A dissociation scheme is proposed to explain the enhancement of the escaping rate by the presence of Xe(1). There are two branches for the CO escaping pathway. The dominant part of the dissociated CO escapes to the solvent through the Xe(1) trapping site under the Xe-free condition, and there are at least three intermediate states along this pathway. When a Xe atom blocks the Xe(1) site, the CO escapes through another route.

1. Introduction

Hemoglobin (Hb) and myoglobin (Mb) carry important biological functions as the oxygen transport and storage in the blood and muscles, respectively. The cooperative interactions among the subunits of Hb are considered to cause an enhancement of the oxygen transport. The protein structural change as well as the ligand dissociation pathway should be key steps in understanding this important protein function. Mb has been used as a model system to clarify these key steps, and, because of this importance in biochemical function, the ligand escaping process from the iron atom in heme of Mb to solvent has attracted many researchers for more than 20 years.[1-45] In

particular, many techniques have been used to identify the pathway for the ligand escaping. It is now almost certain that

(1) Austin, R. H.; Beeson, K. W.; Eisenstein, L.; Frauenfelder, H.; Gunsalus, I. C. *Biochemistry* **1975**, *14*, 5355–5373.
(2) Case, D. A.; Karplus, M. *J. Mol. Biol.* **1979**, *132*, 343.
(3) Beece, D.; Eisenstein, L.; Frauenfelder, H.; Good, D.; Marden, M. C.; Reinish, M. L.; Reynolds, A. H.; Sorensen, L. B.; Yue, K. T. *Biochemistry* **1980**, *19*, 5147.
(4) Henry, E. R.; Sommer, J. H.; Hofrichter, J.; Eaton, W. A. *J. Mol. Biol.* **1983**, *166*, 443–451.
(5) Tilton, R. F., Jr.; Kuntz, I. D., Jr.; Petsko, G. A. *Biochemistry* **1984**, *23*, 2849–2857.
(6) Srajer, V.; Reinisch, L.; Champion, P. M. *J. Am. Chem. Soc.* **1988**, *110*, 6656–6670.
(7) Elber, R.; Karplus, M. *J. Am. Chem. Soc.* **1990**, *112*, 9161–9175.
(8) Xie, X.; Simon, J. D. *Biochemistry* **1991**, *30*, 3682–3692.
(9) Srajer, V.; Champion, P. M. *Biochemistry* **1991**, *30*, 1390–1402.
(10) Champion, P. M. *J. Raman. Spectroscopy* **1992**, *23*, 557–567.
(11) Schlichting, I.; Berendzen, J.; Phillips, G. N., Jr.; Sweet, R. M. *Nature* **1994**, *317*, 808–812.
(12) Teng, T. Y.; Srajer, V.; Moffat, K. *Nat. Struct. Biol.* **1994**, *1*, 701–705.
(13) Hartmann, H.; Zinser, S.; Komninos, P.; Schneider, R. T.; Nienhaus, G. U.; Parak, F. *Proc. Natl. Acad. Sci. U.S.A.* **1996**, *93*, 7013–7016.
(14) Srajer, V.; Teng, T.; Ursby, T.; Pradervand, C.; Ren, Z.; Adachi, S.; Schildkamp, W.; Bourgeois, D.; Wulff, M.; Moffat, K. *Science* **1996**, *274*, 1726.
(15) Vojtchovský, J.; Chu, K.; Berendzen, J.; Sweet, R. M.; Schlichting, I. *Biophys. J.* **1999**, *77*, 2153–2174.
(16) Brunori, M.; Vallone, B.; Cutruzzolá, F.; Travaglini-Allocatelli, C.; Berendzen, J.; Chu, K.; Sweet, R. M.; Schlichting, I. *Proc. Natl. Acad. Sci. U.S.A.* **2000**, *97*, 2058–2063.
(17) Ostermann, A.; Waschipky, R.; Parak, F. G.; Nienhaus, G. U. *Nature* **2000**, *404*, 205–208.
(18) Chu, K.; Vojtchovský, J.; Mcmahon, B. H.; Sweet, R. M.; Berendzen, J.; Schlichting, I. *Nature* **2000**, *403*, 921–923.
(19) Schotte, F.; Lim, M.; Jackson, T. A.; Smirnov, A. V.; Soman, J.; Olson, J. S.; Phillips, G. N., Jr.; Wulff, M.; Anfinrud, P. A. *Science* **2003**, *300*, 1944–1947.
(20) Springer, B. A.; Sriger, S. G.; Olson, J. S.; Phillips, G. N., Jr. *Chem. Rev.* **1994**, *94*, 699–714.
(21) Ansari, A.; Jones, C. M.; Henry, E. R.; Hofrichter, J.; Eaton, W. A. *Biochemistry* **1994**, *33*, 5128–5145.
(22) Lambright, D. G.; Balasubramanian, S.; Decatur, S. M.; Boxer, S. G. *Biochemistry* **1994**, *33*, 5518–5525.
(23) Huang, X.; Boxer, S. G. *Nat. Struct. Biol.* **1994**, *1*, 226–229.
(24) Olson, J. S.; Phillips, G. N., Jr. *J. Biol. Chem.* **1996**, *271*, 17593–17596.
(25) Cansgrove, T. P.; Dyer, R. B. *J. Phys. Chem.* **1996**, *100*, 3273–3277.
(26) Lim, M.; Jackson, T. A.; Anfinrud, P. A. *Nat. Struct. Biol.* **1997**, 209–214.
(27) Scott, E. E.; Gibson, Q. H. *Biochemistry* **1997**, *36*, 11909.
(28) Brunori, M.; Cutruzzolá, F.; Savino, C.; Travaglini-Allocatelli, C.; Vallone, B.; Gibson, Q. H. *Biophys. J.* **1999**, *76*, 1259–1269.
(29) Scott, E. E.; Gibson, Q. H.; Olson, J. S. *J. Biol. Chem.* **2001**, *276*, 5177
(30) Brunori, M.; Gibson, Q. H. *EMBO Rep.* **2001**, *2*, 674–679.
(31) Lamb, D. C.; Nienhaus, K.; Arcovito, A.; Draghi, F.; Miele, A. E.; Brunori, M.; Ulrich Nienhaus, G. *J. Biol. Chem.* **2002**, *277*, 11636–11644.
(32) (a) Mukai, M.; Nakashima, S.; Olson, J. S.; Kitagawa, T. *J. Phys. Chem. B* **1998**, *102*, 3624–3630. (b) Sakan, Y.; Ogura, T.; Kitagawa, T.; Fraunfelter, F. A.; Mattera, R.; Ikeda-Saito, M. *Biochemistry* **1993**, *32*, 5815–5824.
(33) Carver, T. E.; Rohlfs, R. J.; Olson, J. S.; Gibson, Q. H.; Blackmore, R. S.; Springer, B. A.; Sligar, S. G. *J. Biol. Chem.* **1990**, *265*, 20007–20020.
(34) Esquerra, R. M.; Goldbeck, R. A.; Kim-Shapiro, D. B.; Kliger, D. S. *Biochemistry* **1998**, *37*, 17527–17536.
(35) Schlichting, I.; Chu, K. *Curr. Opin. Struct. Biol.* **2000**, *10*, 744–752.
(36) (a) Kleinert, T.; Doster, W.; Leyser, H.; Petry, W.; Schwarz, V.; Settles, M. *Biochemistry* **1998**, *37*, 717–733. (b) Nakashima, S.; Kitagawa, T.; Olson, J. S. *Chem. Phys.* **1998**, *228*, 323–336.
(37) Ishikawa, H.; Uchida, T.; Takahashi, S.; Ishimori, K.; Morishima, I. *Biophys. J.* **2001**, *80*, 1507–1517.

there exist a few distinct intermediate states (the ligand trapped inside the protein interior) along the pathway. Biologically, the ligand trapping pocket inside the protein is considered to be important to protect the heme iron from oxidation by solvent, and the nature of the pocket has been the subject of a number of research projects.

In many cases, the ligand escaping pathway has been studied by using carbon monoxide (CO) as the ligand, because of the near unit probability for CO to escape to solvent. This CO trapping site has been frequently related to cavities observed by X-ray crystallographic measurements.[5] The structures of geminate states at low temperatures have been obtained by several groups, and the results showed that the CO just after the dissociation is located in the vicinity of the heme in the so-called primary docking site,[11–13] although the exact position of the CO is different depending on the literature.[35] The X-ray diffraction study of Mb single crystals with a nanosecond time resolution at room temperature was reported to indicate immediate disappearance of the CO density adjacent to the iron.[14] Subsequent X-ray crystallographic studies showed that the CO migrates away from the primary docking site into internal cavities within the protein known as the xenon trapping sites.[16–19] In particular, two cavities are located on the distal and the proximal sides of the heme.[5] The cavity on the distal side is called Xe(4) and that on the proximal side is called Xe-(1) (Figure 1). The Xe(1) pocket is located underneath the porphyrin ring in a cavity circumscribed by Leu89, Phe138, and Leu14.[5] Lamb et al. used the Fourier transform IR spectroscopy combined with the temperature derivative spectroscopy to observe changes in the dynamics that were attributed to the presence of different docking sites at low temperature.[31] The locations were discussed in terms of the Xe trapping sites. It is now clear that the photodissociated CO is trapped in these cavities, at least, under the crystalline condition at low temperatures.

In the solution phase at physiological temperatures, however, this escaping scheme could be different from that at low temperatures or in the crystalline phase, because of the protein conformational fluctuation, which should be enhanced at higher temperatures in low viscosity liquids. In the solution phase, the ligand dissociation scheme has been intensively investigated mostly on the basis of measurements of geminate recombination kinetics or bimolecular recombination kinetics under various conditions with different temperatures, pHs, and so on for various mutants. Although it has been well-recognized that there are several intermediate states separated by activation barriers along the escaping pathway, the CO escaping process in solution
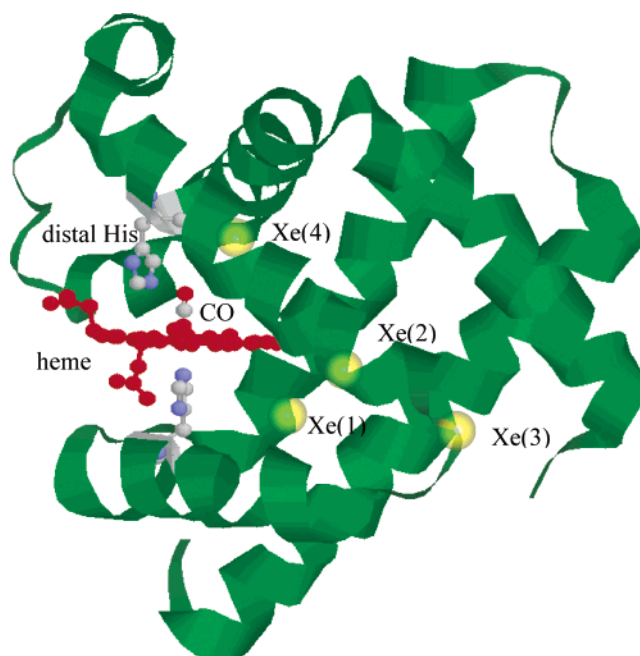
Figure 1. Structure of MbCO. The heme, CO, distal His, and proximal His are shown in ball-and-stick representation. The Xe trapping sits are shown by balls, and names of the positions are also shown (ref 5).

at physiological temperatures has been less clear. To examine the participation of the cavities of the Xe trapping sites for the ligand escape process, studying the Xe effect on the ligand escaping kinetics may be useful. If the CO trapping sites are related to the Xe trapping sites, Xe and the photodissociated CO would compete with each other to occupy them, and the CO escaping kinetics should be altered by the presence of Xe. A thermodynamic analysis of the absorption of Xe by Mb[46] and a crystallographic study[5] have suggested that the Xe(1) site is populated some 10 times more readily than the Xe(4) site. Hence, the contributions of Xe(1) and Xe(4) can be distinguished by varying the partial pressure of Xe. On the basis of this idea, Scott et al. reported on geminate recombination kinetics of oxygen molecule (O_2) for 25 different oxymyoglobin mutants in the presence of 12 atm of Xe.[29] Progressive changes in recombination rates were observed as the pressure was increased. On the basis of the experimental observations, they proposed a dissociation scheme of O_2 from the protein to solvent as described later.

Contrary to the well-studied recombination kinetics, the ligand escaping kinetics has been less clear, because the ligand escaping process from the protein is spectroscopically almost silent when the heme optical transition is monitored. Recently Anfinrud and co-workers reported that the CO escaping to solvent can be detected as a change in the IR absorption band shape and it occurred on a 1-μs time scale.[38] Miller and co-workers[39–42] and our group[43–45] studied the ligand dissociation process by the transient grating (TG) method. The ligand dissociation process from the protein to solvent was traced continuously, and the rate was determined to be 700 ns at 20 °C. The ligand escape rate slower than the apparent geminate recombination rate ($\sim$180 ns)[4] clearly indicates that there is a ligand trapping site inside the protein. A quantitative measurement of the TG signal provided the volume change and released heat within 10 ns (5

(38) Jackson, T. A.; Lim, M.; Anfinrud, P. A. In *Seventh International Conference on Time-Resolved Vibrational Spectroscopy: Proceedings of the conference*; LA-13290-C; Dyer, R. B., Martinez, M. A. D., Shreve, A. P., Woodruff, W. H., Eds.; Los Alamos National Laboratory: Los Alamos, NM, 1995; pp 9–13.
(39) Richard, L.; Genberg, L.; Deak, J.; Chiu, H. L.; Miller, R. J. *Biochemistry* **1992**, *31*, 10703–10715.
(40) Deak, J.; Chiu, H. L.; Lewis, C. M.; Miller, R. J. D. *J. Phys. Chem. B* **1998**, *102*, 6621–6634.
(41) Dadusc, G.; Ogilvie, J.; Schulenberg, P.; Marvet, U.; Miller, R. J. D. *Proc. Natl. Acad. Sci. U.S.A.* **2001**, *98*, 6110–6115.
(42) Ogilvie, J. P.; Plazanet, M.; Dadusc, G.; Miller, R. J. D. *J. Phys. Chem. B* **2002**, *106*, 10460–10467.
(43) Sakakura, M.; Yamaguchi, S.; Hirota, N.; Terazima, M. *J. Am. Chem. Soc.* **2001**, *123*, 4286–4294.
(44) Sakakura, M.; Morishima, I.; Terazima, M. *J. Phys. Chem. B* **2001**, *105*, 10424–10434.
(45) Sakakura, M.; Morishima, I.; Terazima, M. *Biochemistry* **2002**, *41*, 4837–4846.

(46) Ewing, G. J.; Maestas, S. *J. Phys. Chem.* **1970**, *74*, 2341–2344.

mL/mol and 151 kJ/mol, respectively) as well as those associated with the ligand escape process (15 mL/mol and 8 kJ/mol) without any assumption for horse heart and sperm whale MbCO.[42,43] A sequential four state model was used to describe the ligand dissociation reaction at room temperature.[42,44] Furthermore, to obtain an insight into the nature of the intermediate state and of the CO trapping site, the volume difference between the CO trapped Mb and the CO free Mb was measured. It was found that the volume difference is smaller than the partial molar volume of CO in solvents.[45] This fact suggests that CO is trapped in a vacant cavity inside the Mb protein. However, the relation between the CO trapping site and the Xe trapping site was not made clear.

In the present study, the Xe pressure dependence of the *CO escaping* process from the heme to solvent was examined through the molecular volume change by the TG method. We found that the CO escaping rate increased with increasing Xe pressure. The pressure dependence of the rate agrees well with the Xe population at the Xe(1) site. This result clearly indicates that a significant fraction of CO passes through the Xe(1) site in the solution phase at physiological temperatures. We examined several possible dissociation schemes to explain the rate enhancement caused by the Xe occupation at the Xe(1) site and found that the signal features could be explained well based on a branched path model. The volume change of each step for the MbCO containing Xe inside the protein interior is determined by the kinetic analysis based on this scheme.

2. Analysis

The analysis of the TG signal after the photoexcitation of MbCO has been reported previously.[43–45] Briefly, when two laser beams are crossed at an angle θ within the coherence time, an interference (grating) pattern is created with a wavenumber q,[47]

$$q = 4\pi \sin(\theta/2)/\lambda_{ex} \tag{1}$$

where λ_{ex} is the wavelength of the excitation laser light. The MbCO sample is photoexcited by this grating light, and the photodissociation reaction is triggered. When a probe beam is introduced to the interference region, a part of the light is diffracted as a TG signal. The TG intensity (I_{TG}) is proportional to the square of the refractive index (δn) and/or absorbance (δk) differences between the peak-null of the grating pattern[47]

$$I_{TG} = \alpha(\delta n)^2 + \beta(\delta k)^2 \tag{2}$$

where α and β are constants determined by the experimental conditions.

The time-profile of the amplitude (δk) grating is the same as that of the transient absorption signal at the probe wavelength. For the photolysis of MbCO, the time-profile is rather simple: the signal rises quite fast (within our time response), decays slightly (~4% in total amplitude) with a 180-ns lifetime by the geminate recombination, and decays with a 2-ms lifetime by the bimolecular recombination. Since in a previous article we confirmed that the main part of the dynamics of the TG signal in the $0-100$ μs range comes from that of the phase (δn)

(47) Eichler, H. J.; Gunter, P.; Paul, D. W. *Laser-Induced Dynamic Gratings*; Springer-Verlag: Berlin, 1986.

grating,[43–45] we will consider the time dependence of the amplitude grating term only for the bimolecular recombination (vide infra) in this article.

There are several origins for creating the phase grating.[47–52] One of the dominant contributions is the temperature change of the medium induced by the liberated energy from the decay of excited states and by the enthalpy change of the reaction. If the heating process is fast enough to release the thermal energy of Q, the temporal profile is given by[47–52]

$$\delta n_{th}(t) = [(dn/dT)Q/\rho C_p] \exp(-D_{th}q^2 t) = \delta n_{th} \exp(-D_{th}q^2 t) \tag{3}$$

where dn/dT is the temperature dependence of the refractive index, ρ is the density, C_p is the heat capacity at a constant pressure, and D_{th} is the thermal diffusivity. The characteristic rate constant, $D_{th}q^2$, is a good indicator for assigning the signal to the thermal grating.

A newly formed species and the depletion of the original species contribute to the phase grating.[47–52] The component due to the absorption spectrum change is called the population grating. If the molecular volume of the intermediate or the product is different from that of the reactant, the volume change will contribute to the phase grating and is called the volume grating. Sum of these contributions are referred to "the species grating (δn_{spe})" ($\delta n_{spe} = \delta n_{pop} + \delta n_{vol}$, where δn_{pop} and δn_{vol} are the refractive index changes due to the population and the volume gratings, respectively). The magnitude of δn_{spe} of i-th species ($\delta n_{spe}{}^i$) is given by[48]

$$\delta n_{spe}{}^i = \frac{(n_0{}^2 + 2)^2}{6n_0} \frac{1}{3\epsilon_0} \Delta N_i \left(\alpha_i - \frac{\bar{V}_i}{\bar{V}_{solvent}} \alpha_{solvent} \right) \tag{4}$$

where α_i and $\alpha_{solvent}$ are polarizabilities of the i-th species and the solvent molecules, respectively. From this expression, the volume grating term (δn_{vol}) is extracted as[48]

$$\delta n_{vol}{}^i = -\frac{(n_0{}^2 + 2)^2}{18n_0\epsilon_0} \frac{\alpha_{solvent}}{\bar{V}_{solvent}} \Delta N_i \bar{V}_i \tag{5}$$

The species grating signal disappears with a rate constant of Dq^2 (D = diffusion constant of the species) and a recombination reaction with a time constant of k_{rec}. In the case of the MbCO dissociation reaction, MbCO is photodissociated to yield Mb and CO, and then Mb and CO recombine to recover MbCO. Hence, three chemical species—MbCO, Mb, and CO—are involved in the species grating. In this case, the time profile of the species phase grating is expressed by a biexponential function, and it may be given by[41–45]

$$\delta n_{spe} = \delta n_{co} \exp[-(D_{CO}q^2 + k_{rec})t] + \delta n_{Mb} \exp[-(D_{Mb}q^2 + k_{rec})t] \tag{6}$$

where δn_{co} is the refractive index change by the presence of CO, and δn_{Mb} is proportional to the difference between the

(48) Hara, T.; Hirota, N.; Terazima, M. *J. Phys. Chem.* **1996**, *100*, 10194−10200.
(49) Terazima, M. *J. Photochem. Photobiol. C* **2002**, *24*, 1−28.
(50) Terazima, M. *Adv. Photochem.* **1998**, *24*, 255−338.
(51) Nishioku, Y.; Nakagawa, M.; Tsuda, M.; Terazima, M. *Biophys. J.* **2001**, *80*, 2922−2927.
(52) Takeshita, K.; Hirota, N.; Imamoto, Y.; Kataoka, M.; Tokunaga, F.; Terazima, M. *J. Am. Chem. Soc.* **2000**, *122*, 8524−8528.

refractive index changes due to the presence of Mb and of MbCO. Furthermore, D_{CO} and D_{Mb} are the diffusion coefficients of CO and Mb, respectively.

The amplitude grating consists of the periodic grating pattern of a chemical species absorbing the probe light. There should be no contribution due to CO in the amplitude grating signal, because CO possesses no absorption at the probe wavelength. The time profile is given by[43−45]

$$\delta k_{spe} = \delta k_{Mb} \exp[-(D_{Mb}q^2 + k_{rec})t] \tag{7}$$

where δk_{Mb} is proportional to the difference between the absorption changes by Mb and MbCO.

3. Experimental Section

The experimental setup for the TG measurement was reported previously.[43−45] Briefly, in the TG measurement, a laser beam from the second harmonics of a Nd:YAG laser (Spectra Physics, GCR170; $\lambda = 532$ nm; pulse width ∼10 ns) was split into two with a beam splitter and crossed in the sample by a lens (focus length = 20 cm) to create the transient grating. The transient grating was detected as a diffraction of a CW probe beam (diode laser; SDL-5411-G1, 840 nm) that was led into the transient grating region with the angle satisfying the Bragg condition. The diffracted beam (TG signal) was detected by a photomultiplier after passing a pinhole. The signal was averaged by a digital oscilloscope (Tektronics, TDS-520) and a microcomputer. The grating wavenumber, q, was determined from the decay rate of the thermal grating signal and D_{th} (eq 3). The repetition rate of the excitation was 3 Hz, which allows the dissociated Mb to return back to the original MbCO.

Myoglobin from horse muscle was purchased from Nakalai Tesque Co. For preparation of the sample solution, a 10 mM Tris-HCl buffer (pH = 8.0) solution of met Mb was filtered to remove small particles by a membrane filter and was sealed in a cell with a rubber septum. After the dissolved O_2 was purged by flowing nitrogen gas, Fe(III) in the heme of Mb was reduced to Fe(II) by adding sodium dithionite. The solution was then transferred to a stainless steel high-pressure cell[53] having an optical path length of 2 mm with quartz windows under the nitrogen gas condition. The cell was then connected to a gas reservoir. First, 0.1 MPa CO gas and then the required pressure of Xe was introduced to the cell. The pressure of the solution was monitored by a strain gauge (Kyowa PGM-20KH), which was directly connected to the cell. The sample was equilibrated under the mixed gas condition at least for 3 h. To control the temperature of the sample, methanol from a thermostated bath (Lauda RLS6-D) was circulated through the cell. The stage of ligation of the protein was checked by measuring the optical absorption spectrum. The experiments were repeated several times in different days, and averaged values were calculated.

4. Results

4.1. TG Signal without Xe. In this article, we studied the ligand escaping process from the protein interior after the photodissociation reaction of MbCO by monitoring the kinetics and volume changes at various Xe pressures. The TG signal of MbCO in the absence of Xe was described and analyzed in detail in previous articles.[39−45] We first briefly summarize the features of the signal here for a comparison purpose. Figure 2a shows the TG signal of MbCO in a 10 mM Tris buffer solution at 20 °C. The signal rises within the excitation pulse width followed by a decay, a slower rise, and further decay compo-

(53) Saga, N.; Kimura, Y.; Hirota, N.; Terazima, M. *Anal. Sci.* **2001**, *17*, S234236.
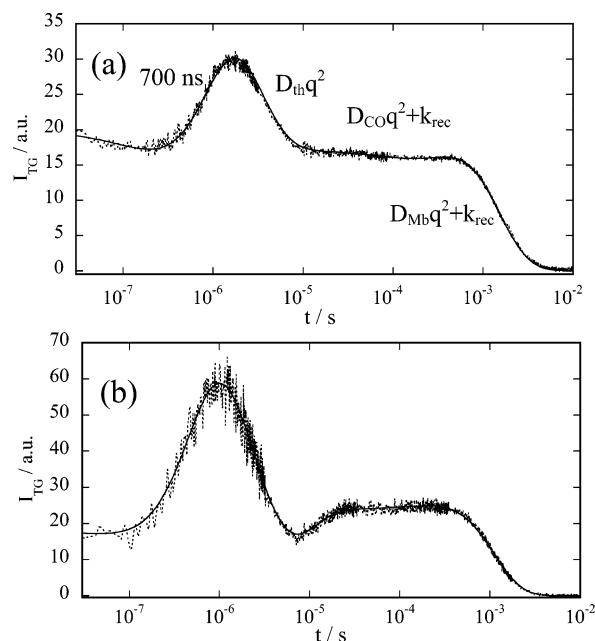
Figure 2. Time profiles of the transient grating signals (dotted lines) after photoexcitation of MbCO in Tris buffer at 20 °C in the presence of (a) 0.1 MPa of carbon monoxide ($q^2 = 1.4 \times 10^{12}$ m^{-2}) and (b) 0.1 MPa of carbon monoxide and 0.9 MPa of xenon ($q^2 = 1.0 \times 10^{12}$ m^{-2}). Various dynamics are apparent in these signals. The rate constants corresponding to these dynamics for (a) are labeled in (a). Continuous solid lines are the best fits using eq 8.

nents. Since the decay rate constant in the 10-μs range agrees well with $D_{th}q^2$ under the present experimental condition, this component should be attributed to the thermal grating signal. The slow rise feature on a submicrosecond time scale comes from the cancellation of the thermal grating signal by a species grating signal with a lifetime of 700 ns. The signal intensity at the bottom of the dip (around ∼100 ns) represents the amplitude grating (δk) signal intensity. From a TG experiment at a large wavenumber, we have previously shown that the signal with the 700-ns kinetics mainly comes from a volume change.[43,44] The slower temporal profile in the ∼submillisecond−millisecond time range can be expressed by a biexponential function; the faster component was attributed to the diffusion of the photodissociated CO (not clearly seen in Figure 2 because of the overlap with the slowest decay component, but more apparent in Figure 2 of ref 43 recorded under a different q-condition), and the slowest decay was assigned to the diffusion of Mb and the recombination process of CO to Mb. The decay rate is about the same as the recombination rate (k_{rec}) observed in a transient absorption signal, because $D_{Mb}q^2$ is much smaller than k_{rec} (∼3 ms) under this condition. The TG signal in this whole time range was fitted with the following equation:[43−45]

$$I_{TG}(t) = \alpha\{\delta n_s \exp(-k_s t) + \delta n_{th} \exp(-D_{th}q^2 t) + \\ \delta n_{co} \exp[-(D_{CO}q^2 + k_{rec})t] + \delta n_{Mb} \exp[-(D_{Mb}q^2 + \\ k_{rec})t]\}^2 + \beta\{\delta k_{Mb} \exp[-(D_{Mb}q^2 + k_{rec})t]\}^2 \tag{8}$$

where the rate constant of k_s is (700 ns)$^{-1}$ at 20 °C, and δn_s, δn_{th}, δn_{CO}, and δn_{Mb} are the refractive index changes due to the 700-ns kinetics, heat releasing, CO, and Mb, respectively. The last term, δk_{Mb}, represents the absorption change at the probe wavelength.

The decay-rise curve in the hundreds of nanoseconds time range is due to the cancellation effect between the δn_{th} and δn_s terms, which indicates that the signs of δn_{th} and δn_s are opposite. Since δn_{th} at this temperature is negative, δn_s should be positive. The decay of the positive refractive index change due to the volume grating indicates that the molecular volume change (ΔV_s) during this process is positive (volume expansion). After this dynamics, there is no cancellation effect between the species grating and the thermal grating signal, indicating that the species grating component just after the CO release is almost zero ($\delta n_{spe} = \delta n_{CO} + \delta n_{Mb} = 0$).[43] This is a result of complete cancellation between the negative δn_{CO} and the positive δn_{Mb}. This complete cancellation should be accidental, because there is no intrinsic reason to make δn_{CO} and δn_{Mb} the same amplitudes. In fact, this cancellation is not observed for sperm whale MbCO, in which $|\delta n_{Mb}|$ is slightly larger than $|\delta n_{CO}|$.[44] (Furthermore, this complete cancellation disappears when Xe is introduced as described later.)

Here, two volume changes have been observed in the TG signal; the faster one, which occurs within a pulse width, is denoted by ΔV_f, and the slower one with a lifetime of submicrosecond (700 ns at 20 °C in Xe-free solution) is denoted by ΔV_s.[43] Although nonexponential behavior was expected for the ligand escape process by possible kinetic heterogeneity, the kinetics was found to be expressed by a single exponential function quite well (section 5.2) in a temperature range of 20−0 °C.[43] This exponential kinetics may reflect a fast structural relaxation of the protein at these temperatures. From a q-dependence measurement in a wide q range, the slow dynamics has been clearly attributed to the ligand escape process from the protein to solvent.[44] It has been shown that the volume change during the 700-ns process is $\Delta V_s = 15 \pm 2$ mL/mol.[43] From a PA measurement, the volume change during the process of MbCO → Mb + CO was determined to be $\Delta V_{total} = 9 \pm 3$ cm^3/mol.[43] Therefore, the volume change within a pulse width was calculated to be $\Delta V_f = -5 \pm 3$ cm^3/mol. The molecular origin of the negative volume change in the process of breaking the Fe−CO bond is not obvious. Previously, we suggested that movement of a water molecule to form the so-called distal water may cause this negative volume change based on some site-directed mutation studies.[45]

4.2. TG Signal with Xe. By an addition of Xe to the solution with 0.1 MPa of CO, the temporal profile of the TG signal changes. For example, the TG signal with 0.9 MPa of Xe is shown in Figure 2b. Several notable changes are summarized as follows.

(a) The rate constant of the decay-rise component with the 700-ns lifetime in the Xe-free solution becomes faster with increasing the Xe pressure. The initial parts of the TG signals at various Xe pressures are depicted in Figure 3 with a linear time scale to show this change clearly.

(b) The amplitude of the decay-rise component with the 700-ns lifetime becomes slightly smaller with increasing Xe pressure. (In Figure 3, this change may not be apparent without a curve fitting, because of the cancellation effect between δn_s and δn_{th}.)

(c) Without Xe, the thermal grating signal decays monotonically to the species grating signal. With increasing Xe pressure,
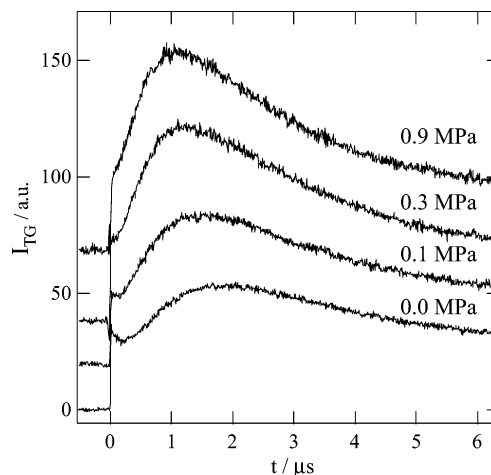
Figure 3. Time profiles of the transient grating signals on linear time scale after photoexcitation of MbCO in Tris buffer at 20 °C at various pressures of xenon ($q^2 = 1.2 \times 10^{12}$ m^{-2}). The pressure of Xe is indicated in the figure. The CO pressure is 0.1 MPa for all samples. The signals are shifted upward with increasing Xe pressure to avoid the overlap. The decay-rise profile for 0 MPa solution is caused by the cancellation of the signals between δn_s and δn_{th} of eq 8.

a dip between the thermal grating and the species grating gradually appears (at around 10 μs under this q^2 condition) (Figure 2b).

(d) The slowest decay rate of the TG signal, which represents the recombination rate and the molecular diffusion rate, gradually increases with increasing Xe pressure.

These changes could be induced by either the effect of the Xe atom or the pressure effect. We examined these possibilities by introducing nitrogen (N$_2$) instead of Xe. When 0.9 MPa of N$_2$ gas was sealed in the sample cell with 0.1 MPa CO, the amplitude of the initial decay component does not change, the rate constant of the rise component is almost the same (680 ns) as that without N$_2$, the dip between the thermal grating and the species grating does not appear, and the recombination rate does not change. The time profile is almost indistinguishable from that without 0.9 MPa of N$_2$ (data is not shown). Therefore, the observed Xe pressure dependence is not due to the pressure effect but to the coexistence of the Xe atom inside the protein.

Furthermore, we examined whether the quantum yield of the CO escape is altered by an addition of Xe. Since the species grating signal due to CO represents the amount of CO escaped from Mb, the signal intensity of this component is a good indicator of the amount of the escaped CO. We measured the relative amplitudes of δn_{CO} at various Xe pressures and found that it did not change by changing the Xe pressure. Hence, the quantum yield of the CO escape is not influenced by the presence of Xe.

The above four changes induced by the presence of Xe can be explained as follows.

(a) The increased k_s means that the CO escape rate from the protein is accelerated by the coexistence of Xe inside the protein. A quantitative analysis of the Xe pressure dependence is described later in this section. This observation should be interpreted in terms of the Xe-dependent CO escaping process and will be discussed in detail in section 5.2.

(b) The initial slow rise feature originates from the cancellation between δn_s and δn_{th}. The amplitude of δn_s is determined mainly by the volume change associated with the CO escape
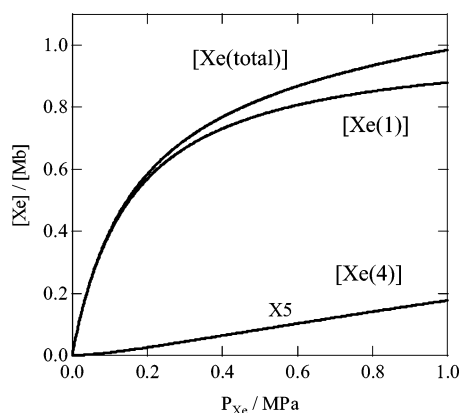
Figure 4. Population of xenon contained in myoglobin ([Xe]/[Mb]) under the pressure of xenon (P_{Xe}) calculated from data of equilibrium constant in ref 46. The total amount of Xe ([Xe(total)]), populations at the Xe(1) site-([Xe(1)]), and Xe(4) site ([Xe(4)]) are shown.

(ΔV_s).[43] Therefore, the decrease in the amplitude of this component indicates that ΔV_s decreases with increasing the Xe pressure. A quantitative analysis of this volume change is discussed in the next section.

(c) Considering that δn_{th} is negative at room temperature, we can explain the appearance of the dip between the thermal grating and species grating signal (at ~10 μs in Figure 2) by a positive increase of δn_{spe} (= $\delta n_{CO} + \delta n_{Mb}$ in eq 8) with increasing Xe pressure. Since the amplitude of δn_{CO} as well as the absorption spectrum of MbCO do not change by the presence of Xe, the increase of δn_{spe} should be attributed to an increase of δn_{vol} due to Mb; i.e., the total volume change (ΔV_{total}) decreases with increasing the Xe pressure. A quantitative analysis of the Xe pressure dependence of this volume change is discussed in the next section.

(d) The decay rate constant of the slowest species grating signal is given by $D_{Mb}q^2 + k_{rec}$ in eq 8. From a q-dependence measurement, we found that the enhancement of the decay rate was due to the acceleration of the bimolecular recombination reaction (k_{rec}). This point will be discussed in section 5.3.

One of the important observations here is that the presence of Xe changes the escaping rate of CO from the protein interior to the solvent at room temperature. If the CO escaping route is not related to the Xe trapping site in the protein, the presence of Xe should not influence the escaping properties. Therefore, we conclude that a significant fraction of CO escapes from the protein through the Xe trapping site at room temperature, at least, in the Xe-free solution. The CO escaping process in the presence of Xe will be discussed in section 5.2.

Several Xe trapping sites were reported.[5] The Xe site that affects the CO escaping process can be identified by measuring the Xe pressure dependence, because the Xe affinities of these sites are different. Two equilibrium constants were reported; the larger one corresponds to the occupation of the Xe(1) site and the other one to the occupation of the other Xe trapping sites.[46] Figure 4 depicts the fraction of Xe-contained Mb calculated from these equilibrium constants reported before.[46] In a range of 0−0.6 MPa, Xe occupies mostly the Xe(1) site and the other sites are almost empty. By comparison with this curve, we analyzed the TG signals at various Xe pressures using the same equation for the signal without Xe (eq 8). This analysis should be an approximate one, because MbCO in a middle pressure range of Xe (where the Xe(1) site is not saturated)
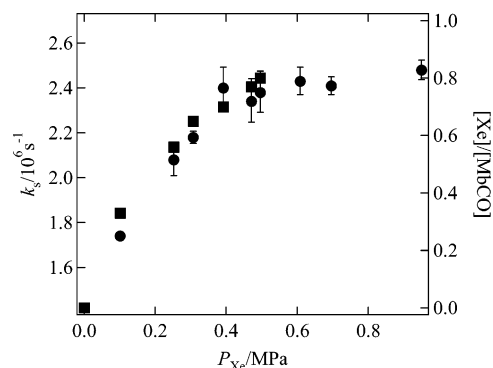
Figure 5. Xe pressure (P_{Xe}) dependence of the apparent CO escaping rate (k_s) from Mb determined by a fitting of the slow rising component (k_s) with eq 8 (squares). The Xe population at the Xe(1) site calculated by the equilibrium constant of Xe in Mb is also shown (circles).
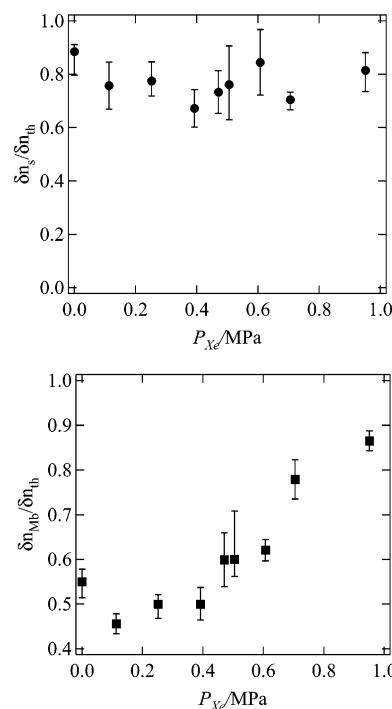
Figure 6. Xe pressure (P_{Xe}) dependence of the refractive index change due to the CO escaping (δn_s in eq 8) and the difference between the refractive index changes by the presence of Mb and MbCO (δn_{Mb} in eq 8). The changes of these refractive indices indicate the volume changes induced by the Xe trapped inside the protein interior.

should be a mixture of MbCO with and without Xe, and the time profile should be analyzed by a sum of contributions from these two species. This analysis will be presented in section 5.2. Here, the profile is preliminarily fitted by a single exponential function (k_s term in eq 8) to show the Xe pressure dependence of the rate constant clearly. The slow rising rate k_s is plotted in Figure 5 together with the relative population of the Xe(1) site. Interestingly, the pressure dependence of k_s agrees well with the Xe population at the Xe(1) site. This result strongly indicates that a significant fraction of CO passes through the Xe(1) trapping site before escaping from the protein under the Xe-free condition.

4.3. Volume Change. The Xe pressure dependence of the amplitude of δn_s normalized by δn_{th} is plotted in Figure 6. As described in the principle section, there are two contributions in the species grating component: population and volume gratings. Since absorption spectra of both MbCO and Mb do

Table 1. Apparent Total Molecular Volume Changes (ΔV_{total}), Apparent Volume Changes Associated with the CO Escape to Solvent (ΔV_s), and Apparent Volume Changes within Our Time Response (~20 ns) ($\Delta V_f = \Delta V_{total} - \Delta V_s$) after Photoexcitation of MbCO at 20 °C at Various Pressures of Xe (P_{Xe})[a]

P_{Xe}/MPa	ΔV_{total}/mL mol^{-1}	ΔV_s/mL mol^{-1}	ΔV_f/mL mol^{-1}
0	9[b]	14.7 ± 1.0	−5 ± 1
0.11	10.7 ± 0.5	12.6 ± 1.0	−3 ± 1
0.25	10.0 ± 0.5	12.9 ± 1.0	−3 ± 1
0.39	10.0 ± 0.5	11.1 ± 1.0	−2 ± 1
0.47	8.1 ± 0.8	12.0 ± 1.0	−4 ± 2
0.51	8.1 ± 0.8	12.6 ± 2.3	−5 ± 3
0.61	8.0 ± 0.5	14.0 ± 2.3	−6 ± 3
0.71	4.6 ± 0.5	11.7 ± 0.5	−7 ± 1
0.95	2.9 ± 0.5	13.5 ± 1.0	−10 ± 1

[a] These volume changes are determined by the analysis using eq 8 assuming that all of the intermediate species in the sample are uniform. [b] This value has been determined in the previous report (ref 43).

not change by the presence of Xe in the present experimental pressure range, the amplitude of the population grating component should not change by the presence of Xe. Hence, from the change of the amplitude of the slow rising component δn_s and eq 5, the volume change associated with the ligand escape process (ΔV_s) at various Xe pressures can be calculated as listed in Table 1. It should be noted that these values are apparent volume changes, which are obtained by assuming that all of the intermediate molecules in the sample are uniform. In reality, as described above, Mb in the solution at a Xe pressure such that the Xe site is not saturated should be a mixture of Mb with Xe and without Xe inside the protein interior. The apparent volume change in this section is an averaged value for the sample at that Xe pressure.

As evident from the observation of (a) in the previous section (Figure 6), this volume change decreases from 14.7 mL/mol without Xe to 13.4 mL/mol in the presence of 0.9 MPa of Xe condition, where the Xe(1) site is almost saturated. A fact that δn_s changes even at 0.1 MPa of Xe (Figure 6) suggests that the Xe dependence of ΔV_s is caused by the occupation of the Xe-(1) site.

As mentioned in the previous section, it has been reported that the absolute value of the refractive index change due to CO (δn_{CO}) is almost the same as that due to Mb (δn_{Mb}) with an opposite sign ($\delta n_{spe} = \delta n_{CO} + \delta n_{Mb} = 0$, $\delta n_{CO} < 0 < \delta n_{Mb}$) under the Xe-free condition.[43] With increasing pressure of Xe, δn_{spe} gradually increases, resulting in the appearance of a dip between the thermal grating and the species grating signals (at ~10 μs in Figure 2). This dip is interpreted in terms of a positive increase of δn_{Mb}, indicating that the total volume change (ΔV_{total}) decreases with increasing Xe pressure as described in (c) in the previous section. The Xe pressure dependence of δn_{Mb} is shown in Figure 6, and apparent ΔV_{total} calculated from the magnitudes of δn_{Mb} are listed in Table 1. Interestingly, δn_{Mb} does not change so much in a range of 0−0.6 MPa and then gradually increases. This behavior sharply contrasts with the Xe pressure dependence of the Xe(1) population (Figure 4). From the relative amplitude of δn_{spe} determined at 0.9 MPa Xe, we found that the total volume change due to Mb (ΔV_{total}) in the presence of Xe is 2.9 ± 0.5 mL/mol. This value is 6 mL/mol smaller than that without Xe. Considering that ΔV_s is rather insensitive to the Xe pressure (Table 1), we should attribute this ΔV_{total} change to the change in ΔV_f, the fast volume change just after the ligand dissociation

from the iron atom of the heme. Therefore, the Xe pressure dependence of Figure 6 indicates that this volume change is not influenced by the presence of Xe at the Xe(1) site, but it is changed by the occupation of Xe in other trapping sites. This observation may be reasonable because the Xe(1) site is on the opposite side of the porphyrin ring to the CO binding side and the long distance may not allow direct influence of Xe to the CO binding site. The origin of the fast volume change was previously suggested as the movement of a water molecule to the distal site.[45] We may speculate that the Xe effect on this fast volume change is caused by the influence of the trapped Xe on the movement of this water molecule.

5. Discussion

5.1. Is Xe Released from Mb? The results described in the previous section indicate that the major part of the dissociated CO is trapped at the Xe(1) site before escaping to solvent at ambient temperature in the Xe-free solution. When Xe is located on the path of the CO escaping, the Xe could possibly be released from the protein to solvent by the collision with CO. We examined this possibility, whether Xe is released from the protein by the photoirradiation. The species grating signal represents the chemical species involved in the photoreaction. If Xe is released, its presence should be detected as a species grating signal due to Xe. To identify the species grating signal, the amplitudes of the species grating signals were calculated from eq 4 for Xe and CO. Using the Lorentz−Lorenz relationship and the molecular volume of CO (35.7 mL/mol)[48] and Xe (42.7 mL/mol),[54] we obtained the ratio of the amplitude of the species grating signal of Xe (δn_{Xe}) to that of CO (δn_{CO}) to be $\delta n_{Xe}/\delta n_{CO} = -0.75$. The difference between δn_{Xe} and δn_{CO} is so large, and even the sign of the refractive index change is different between Xe and CO. Furthermore, D of CO is 3.4×10^{-9} m^2/s,[48] which is more than 5 times larger than D of Xe (0.6×10^{-9} m^2/s).[55] Therefore, if Xe is released from the protein to solvent, the species grating signal due to Xe, which is very much different from that due to CO, should appear.

We carefully examined the species grating signal if this expected Xe signal was observed. However, the species grating signal could be analyzed well by eq 8 with the reported D_{CO}. Furthermore, we tried to reproduce the observed signal by taking into account the species grating signal of Xe, but we found that the Xe component should not be included in the calculation for the best fitting. We conclude that the Xe trapped inside the protein is not released to solvent but only the CO is released.

5.2. Models for CO Escape. On the basis of the analysis of the previous sections, we found that a significant fraction of CO was released to solvent through the Xe(1) trapping site in the Xe-free solution. When Xe is trapped at the Xe(1) site, CO escapes from the protein to solvent faster without releasing the Xe. We may consider the following two possibilities to explain these observations.

(i) In the intermediate state, the CO is co-trapped at the Xe-(1) trapping site with Xe. From this transient state, the CO is released to the solvent but the Xe stays there.

(54) Moore, J. C.; Battlno, R.; Rettlch, T. R.; Handa, Y. P.; Wllhelm, E. *J. Chem. Eng. Data* **1982**, *27*, 22.
(55) Wise, D. L.; Houghton, G. *Chem. Eng. Sci.* **1968**, *23*, 1211.

Scheme I

$$\text{MbCO} \underset{k_1}{\overset{h\nu}{\rightleftharpoons}} \text{Mb:CO} \xrightarrow{k_2} \text{Mb::CO} \xrightarrow{k_3} \text{Mb} + \text{CO}$$

Scheme II

(a)

$$\text{MbCO} \underset{k_1}{\overset{h\nu}{\rightleftharpoons}} \text{Mb:CO} \underset{k_{-2}}{\overset{k_2}{\rightleftharpoons}} \text{Mb} + \text{CO}$$

$$k_{-3} \updownarrow k_3$$

$$\text{Mb::CO}$$

(b)

$$\text{MbCO} \underset{k_1}{\overset{h\nu}{\rightleftharpoons}} \text{Mb:CO} \underset{k_{-2}}{\overset{k_2}{\rightleftharpoons}} \text{Mb:::CO} \xrightarrow{k_4} \text{Mb} + \text{CO}$$

$$k_{-3} \updownarrow k_3$$

$$\text{Mb::CO}$$

(c)

$$\text{MbCO} \underset{k_1}{\overset{h\nu}{\rightleftharpoons}} \text{Mb:CO} \xrightarrow{k_2} \text{Mb::CO} \xrightarrow{k_4} \text{Mb} + \text{CO}$$

$$k_{-3} \updownarrow k_3$$

$$\text{Mb:::CO}$$

Scheme III

$$\text{MbCO} \underset{k_1}{\overset{h\nu}{\rightleftharpoons}} \text{Mb:CO} \xrightarrow{k_2} \text{Mb::CO} \xrightarrow{k_5} \text{Mb} + \text{CO}$$

$$k_3 \searrow \qquad \nearrow k_4$$
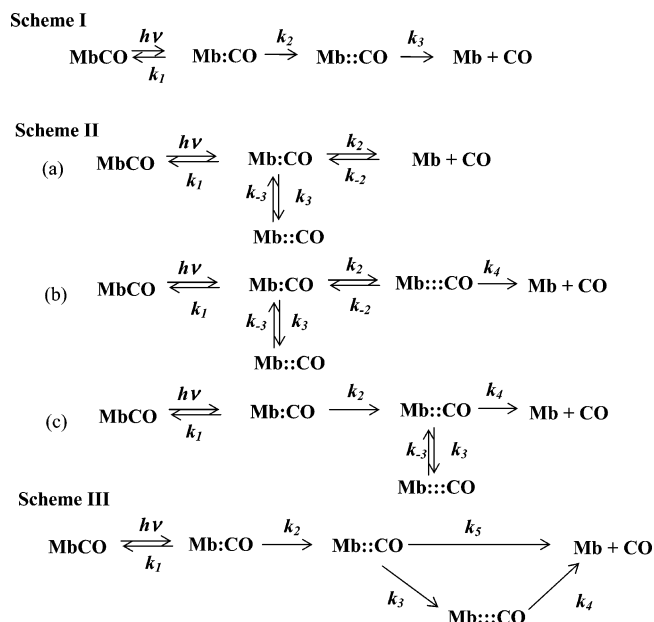
$$\text{Mb:::CO}$$

Figure 7. Kinetic schemes representing CO escaping process from the protein interior. MbCO denotes carboxymyoglobin. Mb:CO, Mb::CO, and Mb:::CO represent different intermediate species.

(ii) The route of the CO escaping in the presence of the Xe is different from that in the absence of Xe. In other words, the main escaping route of CO is changed by the presence of the Xe.

In case (i), the CO is trapped inside the cavity with the Xe. The size of the Xe(1) site cavity is estimated to be about 50 mL/mol,[56] and the partial molar volumes of CO and Xe are 35.7[48] and 42.7 mL/mol,[54] respectively. Hence, MbCO should expand dramatically if both CO and Xe are trapped together. Because of this expansion, the volume change associated with the CO release from the cavity is expected to be a large negative. On the other hand, our experimental result shows that the volume change associated with the ligand escape at 0.9 MPa of Xe (13.5 mL/mol) is not so different from that without Xe (14.7 mL/mol). Therefore, we can exclude this possibility. The CO escaping route should be changed by occupying the Xe site.

We will then consider the CO escaping pathway based on several schemes (Figure 7). The photodissociation of MbCO generates a product called the primary species (Mb:CO). Scheme I is so-called the sequential model; Mb:CO disappears by returning to MbCO or by the conversion to the secondary species (Mb::CO). The CO escapes to solution from this species. Scheme II involves dead-end models. In Scheme IIa, CO escapes to the exterior from Mb:CO. The secondary species (Mb::CO) is formed from Mb:CO and returns to Mb:CO to escape from the protein interior. Scheme III is a branched path model. It is similar to Scheme II, but there are two escaping routes: the ligand escape occurs not only from the Mb::CO state but also from the Mb:::CO state.

(A) Scheme I. In Scheme I, Xe would fill internal spaces along the CO escape route (Mb::CO). Consequently, the fraction of the geminate recombination would be expected to increase and the escape rate to decrease. However, experimentally, an addition of Xe results in no change in the geminate recombina-

(56) Tilton, R. F., Jr.; Singh, U. C.; Weiner, S. J.; Connolly, M. L.; Kuntz, I. D.; Kollman, P. A. *J. Mol. Biol.* **1986**, *192*, 443.

tion yield and an increase in the escaping rate. Therefore, this scheme cannot explain the observations. It is important to emphasize that not only this scheme but also any other sequential scheme cannot explain the observations in this study.

A clue to the solution of the CO escaping scheme is that the CO escaping rate increases with increasing the Xe pressure. When Xe blocks one of the CO escaping routes, the CO is released faster through another route. This observation indicates that the rate through this by-path route is faster than that through the "normal" route, which is used by Mb without Xe. Why does the CO not use the faster route to escape under the Xe-free condition instead of the normal one? This naïve question may be answered by considering a rather stable CO trapping site. If this stable site is formed faster than the escape rate through the by-path route, the CO is released from this trapped site exclusively without taking the by-path route. When Xe blocks this site, the CO should escape to solvent through the by-path route. If the CO releasing rate from this site is slower (700 ns) than the by-path route (400 ns), the observed feature can be explained. In other words, the Xe trapping site should act as the CO trapping site to retard the CO releasing. We may consider two typical models to satisfy above conditions: dead-end models (Scheme II) and a branched path model (Scheme III). Under a condition of 0.9 MPa of Xe, Xe is trapped at the site of Mb::CO in Scheme IIa and b and Mb:::CO in Schemes IIc and III.

(B) Scheme II. Scott et al. investigated the oxygen dissociation scheme by observing the Xe pressure dependence of the geminate recombination rates, and Scheme IIa was proposed.[29] When Xe is introduced into the sample, Xe is trapped in a cavity where CO is trapped in Mb::CO. The time profile of the TG signal based on this scheme is calculated by the following kinetic-diffusion equations:

$$\frac{\partial[\text{MbCO}]}{\partial t} = D_{\text{MbCO}}\frac{\partial^2[\text{MbCO}]}{\partial x^2} + k_1[\text{Mb:CO}]$$

$$\frac{\partial[\text{Mb:CO}]}{\partial t} = D_{\text{Mb:CO}}\frac{\partial^2[\text{Mb:CO}]}{\partial x^2} - (k_1 + k_2 + k_3)[\text{Mb:CO}] + k_{-2}[\text{Mb}][\text{CO}] + k_{-3}[\text{Mb::CO}]$$

$$\frac{\partial[\text{Mb::CO}]}{\partial t} = D_{\text{Mb::CO}}\frac{\partial^2[\text{Mb::CO}]}{\partial x^2} + k_3[\text{Mb:CO}] - k_{-3}[\text{Mb::CO}]$$

$$\frac{\partial[\text{Mb}]}{\partial t} = D_{\text{Mb}}\frac{\partial^2[\text{Mb}]}{\partial x^2} + k_2[\text{Mb::CO}] - k_{-2}[\text{Mb}][\text{CO}]$$

$$\frac{\partial[\text{CO}]}{\partial t} = D_{\text{CO}}\frac{\partial^2[\text{CO}]}{\partial x^2} + k_2[\text{Mb::CO}] - k_{-2}[\text{Mb}][\text{CO}] \quad (9)$$

These equations are solved with an assumption that the diffusion process of all species and the bimolecular recombination reaction are negligible in the time scale for the ligand escape. This assumption is satisfied under this experimental condition, since the molecular diffusion process is on an order of millisecond time range (>10 ms) for $q \approx 10^6$ m^{-1} and the bimolecular recombination reaction time (k_{-2}^{-1}) is 3 ms, while the ligand escaping time is on an order of 700 ns. Solving these equations,

one obtains the build up time profile of the species grating signal as

$$\delta n_{\mathrm{spe}}(t) = \delta n_{\mathrm{Mb:CO}}[\mathrm{Mb{:}CO}] + [\delta n_{\mathrm{Mb:CO}} + (\partial n/\partial V)\Delta V_1 \Delta N]$$
$$[\mathrm{Mb{::}CO}] + [\delta n_{\mathrm{Mb:CO}} + (\partial n/\partial V)(\Delta V_1 + \Delta V_2)\Delta N][\mathrm{Mb}][\mathrm{CO}]$$

$$= \delta n_{\mathrm{A}} \exp(-k_{\mathrm{A}}t) + \delta n_{\mathrm{B}} \exp(-k_{\mathrm{B}}t) + \delta n_{\mathrm{C}} \qquad (10)$$

where

$$\delta n_{\mathrm{A}} = -\frac{k_1(k_1 + k_2 - k_{-3} - F) - k_2 k_3}{2F(k_1 + k_2)} \times \delta n_{\mathrm{Mb:CO}} +$$
$$\frac{k_3}{2F}\Big(\frac{\partial n}{\partial V}\Big)\Delta V_1 \Delta N + \frac{k_1 + k_2 - k_3 - k_{-3} - F}{2F} \frac{k_2}{k_1 + k_2}\Big(\frac{\partial n}{\partial V}\Big)\Delta V_2 \Delta N$$

$$\delta n_{\mathrm{B}} = \frac{k_1(k_1 + k_2 - k_{-3} + F) - k_2 k_3}{2F(k_1 + k_2)} \times \delta n_{\mathrm{Mb:CO}} -$$
$$\frac{k_3}{2F}\Big(\frac{\partial n}{\partial V}\Big)\Delta V_1 \Delta N - \frac{k_1 + k_2 - k_3 - k_{-3} + F}{2F} \frac{k_2}{k_1 + k_2}\Big(\frac{\partial n}{\partial V}\Big)\Delta V_2 \Delta N$$

$$\delta n_{\mathrm{C}} = \Big(\frac{-k_1}{k_1 + k_2}\Big)\delta n_{\mathrm{Mb:CO}} + \frac{k_2}{k_1 + k_2}\Big(\frac{\partial n}{\partial V}\Big)\Delta V_2 \Delta N$$

$$F = \sqrt{(k_1 + k_2 + k_3 - k_{-3})^2 + 4k_3 k_{-3}}$$

$$k_{\mathrm{A}} = \frac{k_1 + k_2 + k_3 + k_{-3} - F}{2}$$

$$k_{\mathrm{B}} = \frac{k_1 + k_2 + k_3 + k_{-3} + F}{2}$$

Here, $\delta n_{\mathrm{Mb:CO}}$ is the refractive index change associated with the MbCO → Mb:CO process, ΔV_1 and ΔV_2 are volume changes by Mb:CO → Mb::CO and Mb:CO → Mb + CO, respectively. Furthermore, ΔN is the number density of the photodissociated MbCO under the Xe-free condition. We assume that the population grating terms for Mb:CO, Mb::CO, and Mb::CO are the same, which is a reasonable assumption because the absorption spectrum is not sensitive to the ligand trapped position. The rate constants, k_{A} and k_{B}, correspond to the ligand escape rate ($(700\ \mathrm{ns})^{-1}$) and the geminate recombination rate ($(180\ \mathrm{ns})^{-1}$), respectively.

Before considering the Xe effect, we estimate the order of the rate constants qualitatively based on the experimental observations without Xe. According to eq 10, the CO release process should be expressed by a biexponential function. On the other hand, as described in the previous article[43] and in section 4.1, this kinetics is well-expressed by a single exponential function with a rate of $(700\ \mathrm{ns})^{-1}$. In Figure 8, we show the initial part of the TG signal in the absence of Xe, which represents the CO escaping process and the decay of the thermal grating, together with the best fitted curve by a single exponential function convoluted with the thermal grating signal. The agreement of the fitting is quite good. To reproduce this single exponential behavior based on Scheme IIa, we must consider that k_3 is much larger than the other rate constants ($k_3 \gg k_{-3}, k_2, k_{-2}$) and k_{-3} is the rate determining rate ($(700\ \mathrm{ns})^{-1}$) for the ligand escape process. Under this condition, δn_{A} becomes dominant compared with δn_{B}. Qualitatively, most of the photodissociated CO is trapped at Mb::CO efficiently and the escape process is determined by the k_{-3} process so that the CO
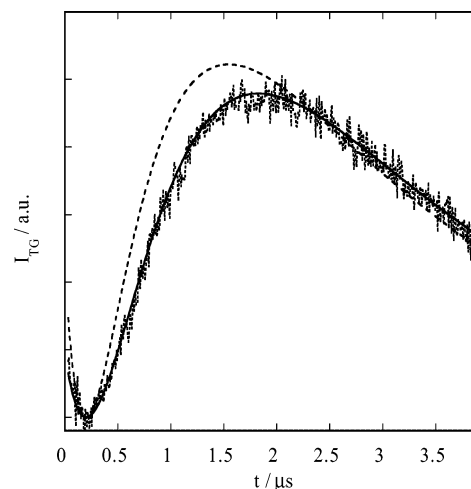
Figure 8. TG signal representing the CO releasing process without Xe is amplified (dotted line) and fitted by a single exponential function with the 700-ns lifetime (solid line) and a biexponential function with lifetimes of 700 and 400 ns (broken line) (based on Scheme IIb of Figure 7) convoluted with the thermal grating signal.

escape process is expressed by a single exponential function well. At the same time, to explain the high escaping yield (94%), the CO should be quickly released from Mb (not returns back to MbCO) after the CO is transferred from Mb::CO to Mb:CO, and this condition can be satisfied by $k_2 \gg k_1$. Hence, the features of the escape process can be reproduced well on the basis of this model with these rate constants.

However, this model with the above-mentioned rate constants cannot account for the Xe pressure dependence. When the Xe-(1) site is occupied by Xe, the Mb:CO → Mb::CO process is blocked. Hence, the k_3 and k_{-3} processes become negligible. In this case, the ligand escape rate should be $k_{\mathrm{B}} \approx (180\ \mathrm{ns})^{-1}$. This is qualitatively understandable, because the CO escape rate of Scheme IIa should be the same as the geminate recombination rate without the CO storage site (Mb::CO). At a Xe pressure such that the Xe(1) site is not saturated, Mb in the solution should be a mixture of Mb containing Xe(1) and without Xe. The observed escaping profile should be expressed by a sum of the escape profiles from these two species:

$$(1 - f)\delta n_{\mathrm{s}} \exp(-k_{\mathrm{s}}t) + f\delta n_{\mathrm{B}}^{\mathrm{Xe}} \exp(-k_{\mathrm{B}}t) \qquad (11)$$

where f is a fraction of the Xe-contained Mb. Furthermore, δn_{s} and k_{s} are parameters in eq 8 for MbCO without Xe, and $\delta n_{\mathrm{B}}^{\mathrm{Xe}}$ is the refractive index change due to the ligand escape for MbCO with Xe. We tried to fit the observed profile using eq 11 with f calculated from the equilibrium constant at the Xe pressure (0.3 MPa, $f = 0.67$),[46] but the calculated one cannot reproduce the observed curve as shown in Figure 9. Therefore, the dynamics from Scheme IIa cannot explain the observed Xe pressure dependence of the rise profile of the TG signal. The poor agreement is due to the large rate constant of k_{B}.

It may be instructive to consider possible modifications within the framework of the dead-end model for reproducing the 400-ns dynamics of the Xe-trapped MbCO. A simple improvement of Scheme IIa may be achieved by placing one more intermediate before the CO releasing step as shown in Scheme IIb. If Mb::CO is blocked by Xe and k_4 is $(400\ \mathrm{ns})^{-1}$ in this scheme, the CO releasing rate with Xe is expected to be 400 ns, which agrees with the experimental observation. However, in this case,
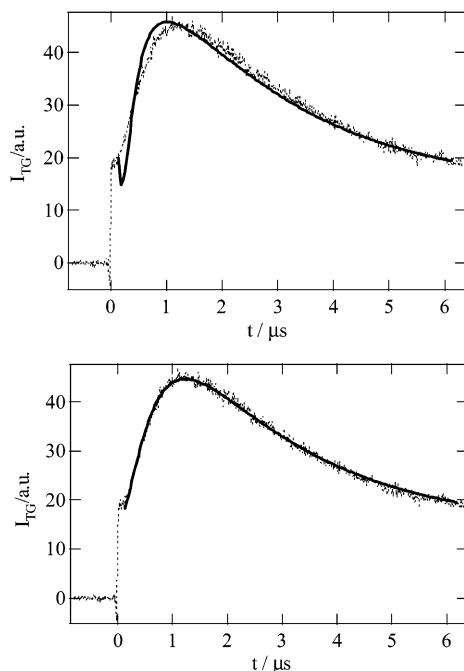
Figure 9. Examples of the best fitted lines (solid lines) for the transient grating signal (dotted lines) due to the CO escaping process in the presence of 0.1 MPa of carbon monoxide and 0.3 MPa of xenon based on Schemes IIa (upper) and III (lower) of Figure 7.

we meet another difficulty: the CO releasing process without Xe cannot be reproduced as follows. The escape process, in this case, should occur from Mb:::CO, which is formed in 700 ns and decays with 400 ns ($= k_4^{-1}$); that is, the CO releasing process is expected to be expressed by a biexponential function of these rate constants with similar amplitudes. We tried to fit the rise part of the TG signal without Xe by this biexponential function, but it was unsuccessful (Figure 8). The origin of the poor fitting is due to the fact that the 400-ns dynamics is too fast to reproduce the rise part for the Xe-free sample.

Another plausible modification of the dead-end model is given as shown in Scheme IIc by adding one more intermediate before a branched intermediate. The reported X-ray structures suggested that the Xe(4) site might be this secondary intermediate site for CO between the primary docking site and the Xe(1) site.[16−19] However, this model cannot explain the observed CO escape process either as follows. To explain the high escaping yield, k_2 should be larger than k_1 ($k_2 \gg k_1$) so that the geminate recombination rate (k_2) should be $(180 \text{ ns})^{-1}$. Using these rate constants, one may find that k_4 should be $(400 \text{ ns})^{-1}$ to explain the kinetics with Xe. However, in this case, the CO escaping process without Xe should be expressed by a convolution of k_{-3} and k_4 ($\sim(400 \text{ ns})^{-1}$); that is, the biexponential function with 400 ns and $\sim$700 ns. This function cannot reproduce the observed TG curve without Xe as stated above for Scheme IIb. Therefore, we can exclude this scheme as well.

It is difficult to make more complex schemes within this dead-end model to simultaneously satisfy the single exponential behavior for the Xe-free sample and the buildup profile under the Xe-trapped condition. Furthermore, it could be difficult to examine the adequacy of such models based on the present experimental results. Although we cannot completely exclude the dead-end model from this experiment, it may be reasonable to conclude that simple dead-end models cannot explain the experimental observations.

(C) Scheme III. Finally we consider Scheme III. The kinetic-diffusion equations based on this scheme are given by:

$$\frac{\partial[\text{MbCO}]}{\partial t} = D_{\text{MbCO}}\frac{\partial^2[\text{MbCO}]}{\partial x^2} + k_1[\text{Mb:CO}]$$

$$\frac{\partial[\text{Mb:CO}]}{\partial t} = D_{\text{Mb:CO}}\frac{\partial^2[\text{Mb:CO}]}{\partial x^2} - (k_1 + k_2)[\text{Mb:CO}] + k_6[\text{Mb}][\text{CO}]$$

$$\frac{\partial[\text{Mb::CO}]}{\partial t} = D_{\text{Mb::CO}}\frac{\partial^2[\text{Mb::CO}]}{\partial x^2} + k_2[\text{Mb:CO}] - (k_3 + k_5)[\text{Mb::CO}]$$

$$\frac{\partial[\text{Mb:::CO}]}{\partial t} = D_{\text{Mb:::CO}}\frac{\partial^2[\text{Mb:::CO}]}{\partial x^2} + k_3[\text{Mb::CO}] - k_4[\text{Mb:::CO}]$$

$$\frac{\partial[\text{Mb}]}{\partial t} = D_{\text{Mb}}\frac{\partial^2[\text{Mb}]}{\partial x^2} + k_4[\text{Mb:::CO}] + k_5[\text{Mb::CO}] - k_6[\text{Mb}][\text{CO}]$$

$$\frac{\partial[\text{CO}]}{\partial t} = D_{\text{CO}}\frac{\partial^2[\text{CO}]}{\partial x^2} + k_4[\text{Mb:::CO}] + k_5[\text{Mb::CO}] - k_6[\text{Mb}][\text{CO}] \quad (12)$$

These equations are solved under the same assumptions for solving eq 9. The buildup time profile of the species grating signal is given by

$$\delta n_{\text{spe}}(t) = \delta n_{\text{Mb:CO}}[\text{Mb:CO}] + [\delta n_{\text{Mb:CO}} + (\partial n/\partial V)\Delta V_1 \Delta N][\text{Mb::CO}] + [\delta n_{\text{Mb:CO}} + (\partial n/\partial V)(\Delta V_1 + \Delta V_2)\Delta N][\text{Mb:::CO}] + [\delta n_{\text{Mb:CO}} + (\partial n/\partial V)(\Delta V_1 + \Delta V_2 + \Delta V_3)\Delta N][\text{Mb}][\text{CO}]$$

$$= \delta n_A \exp(-k_A t) + \delta n_B \exp(-k_B t) + \delta n_C \exp(-k_C t) + \delta n_D \quad (13)$$

where

$$\delta n_A = \frac{k_A - k_2}{k_A}\delta n_{\text{Mb:CO}} - \frac{k_2}{k_A}\left(\frac{\partial n}{\partial V}\right)\Delta V_1 \Delta N + \frac{k_2 k_B}{(k_A - k_B)k_A}\left(\frac{\partial n}{\partial V}\right)\Delta V_2 \Delta N - \frac{k_2(k_4 k_B - k_5 k_A)}{(k_A - k_B)(k_A - k_4)k_A}\left(\frac{\partial n}{\partial V}\right)\Delta V_3 \Delta N$$

$$\delta n_B = -\frac{k_2}{k_A - k_B}\left(\frac{\partial n}{\partial V}\right)\Delta V_2 \Delta N + \frac{k_2(k_4 - k_5)}{(k_A - k_B)(k_B - k_4)}\left(\frac{\partial n}{\partial V}\right)\Delta V_3 \Delta N$$

$$\delta n_C = \frac{k_2 k_3}{(k_A - k_4)(k_B - k_4)}\left(\frac{\partial n}{\partial V}\right)\Delta V_3 \Delta N$$

$$\delta n_D = \left\{\delta n_{\text{Mb:CO}} + \left(\frac{\partial n}{\partial V}\right)\Delta V_{\text{total}}\Delta N\right\}\frac{k_2}{k_A}$$

$$k_A = k_1 + k_2$$

$$k_B = k_3 + k_5$$

$$k_C = k_4$$

Furthermore, ΔV_1, ΔV_2, and ΔV_3 denote the volume changes associated with the processes, Mb:CO → Mb::CO, Mb::CO → Mb:::CO, and Mb:::CO → Mb + CO, respectively.

Apparently, k_A is the geminate recombination rate constant ($\sim(180 \text{ ns})^{-1}$). Since the Xe trapping site is assumed to be the site for Mb:::CO (vide supra) and the CO escaping pathway changes depending on the Xe blocking of the cavity, most of the CO should escape to the solvent from the Mb:::CO state under the Xe-free condition, indicating that k_3 should be much larger than k_5 ($k_3 \gg k_5$). Furthermore, since the 700-ns dynamics has been clearly identified as the CO escaping process from the protein,[44] $k_C = k_4$ should be $(700 \text{ ns})^{-1}$ under the Xe-free condition.

Using this model, we expect that the CO releasing process is expressed by the triexponential function (eq 13). However, if k_3 is much larger than k_A, k_C, and k_5 ($k_3 \gg k_A$, k_C, k_5) and ΔV_3 is also much larger than ΔV_1 and ΔV_2 ($\Delta V_3 \gg \Delta V_1$, ΔV_2), only the $\delta n_C \exp(-k_C t)$ term becomes dominant with the other terms being negligibly small. In this case, the buildup time profile is well-expressed by a single exponential function ($\delta n_s \exp(-k_s t)$ in eq 8) for the Xe-free solution, which agrees with the experimental observation. The smaller volume changes for ΔV_1 and ΔV_2 are reasonable, because they are associated with the CO transfer inside the protein interior, while ΔV_3 should be large because it is associated with the CO releasing process to solvent. Therefore, the single exponential behavior for the Xe-free sample can be explained on the basis of this model.

Importantly, under the above condition, we can simultaneously explain the enhancement of the CO releasing rate with Xe as follows. When Xe is occupied at the Xe(1) site, the Mb::CO → Mb:::CO process is prohibited so that the k_3 and k_4 processes can be neglected. In this case, the $\delta n_C \exp(-k_C t)$ term becomes negligible and the $\delta n_B \exp(-k_B t)$ term becomes dominant as expected from eq 13. The observed CO escaping profile should be expressed by a sum of escape profile from Xe-free MbCO and Xe-contained MbCO as
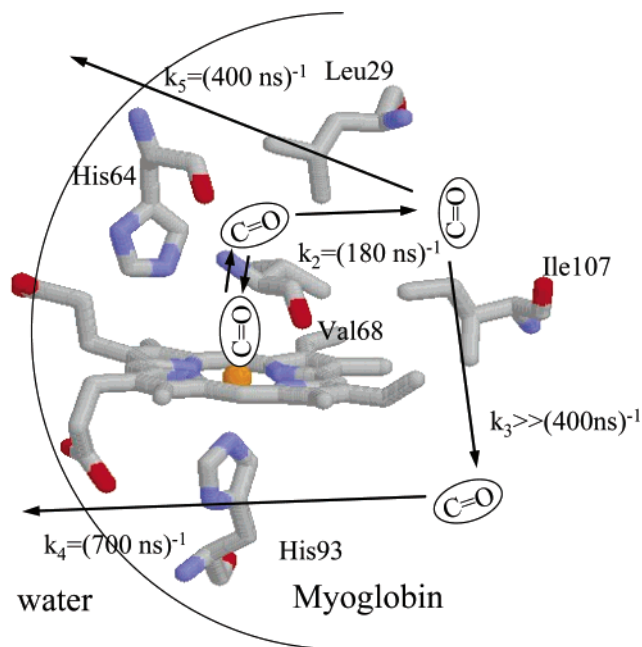
$$(1 - f)\delta n_s \exp(-k_s t) + f\delta n_B^{Xe} \exp(-k_5 t) \qquad (14)$$

We found that the observed signals at various Xe pressures can be consistently reproduced by this equation. It is important to note that adjustable parameters in this equation are only δn_B^{Xe} and k_5. The fraction f is also calculated independently from the reported equilibrium constant,[46] and δn_s and k_s determined for the Xe-free solution are used. For example, the data at 0.3 MPa Xe pressure can be analyzed well as shown in Figure 9 with $f = 0.67$. The best fitted parameters are $k_5 = (2.51 \pm 0.03) \times 10^6 \text{ s}^{-1} = (398 \pm 4 \text{ ns})^{-1}$, and $\Delta V_2 + \Delta V_3 = 13 \pm 1$ mL/mol. We fitted the signals under various pressures of Xe, and the obtained parameters for MbCO containing Xe are listed in Table 2. The obtained parameters agree well with each other, indicating that this scheme can explain the observed TG signal consistently at any pressure of Xe. Therefore, we conclude that this branched path model may be appropriate for describing the CO releasing.

5.3. CO Escaping Process. Using Scheme III, we now describe a molecular model for the CO escaping process. We may safely consider that the CO is located close to the heme (primary docking site) in the initial intermediate Mb:CO as observed by the time-resolved X-ray study[14] and IR spectroscopy.[26] The CO may be then transferred to the other site such as the Xe(4) site in the Mb::CO state. The CO is released from

Table 2. Total Molecular Volume Changes (ΔV_{total}), Volume Changes Associated with the CO Escape to Solvent (ΔV_s), and Volume Changes within Our Time Response ($\sim$20 ns) (ΔV_f) after Photoexcitation of MbCO That Contains Xe at the Xe(1) Site at 20 °C at Various Pressures of Xe (P_{Xe}) Determined by the Analysis Based on Scheme III of Figure 7

P_{Xe}/MPa	ΔV_{total}/mL mol^{-1}	ΔV_s/mL mol^{-1}	ΔV_f/mL mol^{-1}
0.11	5 ± 2	15 ± 2	-10 ± 2
0.25	5 ± 2	13 ± 1	-8 ± 2
0.51	5 ± 2	13 ± 1	-8 ± 2
0.95	3 ± 2	13 ± 1	-10 ± 1

Figure 10. Schematic representation of the CO escaping process from the heme site to solvent. The photodissociated CO from the heme first moves into the empty space near the heme binding site (Mb:CO). Most of CO moves further into a cavity in the protein (Mb::CO), probably at Xe(4) site, with a quantum yield of 94%. This rate constant (k_2) is about (180 ns)$^{-1}$ as observed in the transient absorption signal. Minor fraction of the CO moves back to the heme as the geminate recombination. From this Mb::CO state, the CO can escape the solvent with a lifetime of about 400 ns (k_5^{-1}), but most of them are trapped at the Xe(1) site (Mb:::CO) much faster ($k_3 \gg k_5$). The CO can escape from this site to the solvent with a lifetime of 700 ns (k_4^{-1}).

this site to solvent with a lifetime of $k_5^{-1} = 400$ ns, but the transfer rate to the Xe(1) site (k_3) is much faster so that most of CO is trapped in the Xe(1) site. The CO escapes to solvent from this trapping site directly with a lifetime of 700 ns. When the Xe(1) site is occupied by Xe, the CO cannot go to the Mb:::CO site and escapes through the Mb::CO state with a lifetime of 400 ns. This is a qualitative explanation why CO does not take a faster route without Xe. The ligand escaping process is schematically shown in Figure 10.

Previously, the time-dependent Hartree method was used to predict the ligand escaping trajectory in Mb.[7] The calculation showed that the CO exits by diffusive hopping from one cavity to another in the protein. The multiple sites shown in Figure 10, in particular the Xe(1) site observed in the present experiment, agree with the cavities in this calculation. The calculation also showed multiple exits by ligand trajectories, such as EF and N terminal exit, A/E exit, AB/G exit, proximal His exit, and CD exit.[7] The routes in Figure 10 may indicate these possible exit routes. For example, the exit from the Mb:::

CO site corresponds to the proximal His exit, and the exit from Mb::CO represents the other routes from the distal His side. Recently, a time-resolved X-ray crystallographic study revealed that CO in the Xe(4) site is very short-lived and CO is mostly trapped at the Xe(1) site for about 3 μs.[19] This is also consistent with the present scheme and the assignment that the CO location in Mb::CO and Mb:::CO correspond to the Xe(4) and Xe(1) sites, respectively, although the lifetime of the Xe(1) site is much shorter (700 ns) in solution. For understanding the molecular mechanism of the reversible oxygenation of Hb and Mb in vivo, the ligand dissociation route should be clarified under physiological conditions. The present ligand escaping route based on the investigation under physiological conditions should be useful for further studies of this mechanism.

Finally, we briefly comment on the bimolecular recombination reaction of Mb and CO. The decay rate of the final step of the TG signal represents the molecular diffusion and recombination reaction ($D_{Mb}q^2 + k_{rec}$). This rate slightly increases with increasing the Xe pressure. Since it is hard to believe that the dissolved Xe changes the diffusion coefficient, this rate increase is explained by an increase of k_{rec}. Indeed, by changing q^2, we found that k_{rec} increases from 3 ms without Xe to about 2 ms with 0.9 MPa of Xe. This Xe pressure dependence suggests that the Xe-trapped site (Mb:::CO in Scheme III) is involved also as the route for the CO recombination. If we assume that the CO returns back to the heme position by taking the same route as the escape route (Scheme III), we can explain the observed Xe pressure dependence as follows. Since Mb:::CO acts as the CO storage in the CO recombination process without Xe, the rate from Mb + CO to Mb:::CO should be much faster than that to Mb::CO. The increase in the rate with the Xe pressure increase can be explained if the rate from Mb + CO to Mb::CO is faster ($\sim$(2 ms)$^{-1}$) than that from Mb:::CO to Mb::CO ($\sim$(3 ms)$^{-1}$). This interpretation is similar to that used for the CO escape reaction described above. However, at present, there is no obvious reason to believe that the CO returns back to the heme through the same route as the escaping. We have to discuss this point based on a more detailed study of the recombination process in future. Furthermore, we believe that the CO releasing process may be revealed in more detail by measuring the Xe pressure dependence of the releasing rate for some site-directed mutants.

Conclusion

The CO escaping process from Mb to solvent is studied as a function of Xe pressure under physiological conditions by the time-resolved transient grating technique. We found that the apparent ligand escaping rate and the apparent volume contraction associated with the ligand escape increase with increasing Xe pressure. The pressure dependence of the rate agrees well with the expected Xe population at the Xe(1) site. This result clearly indicates that a significant fraction of the dissociated CO passes through the Xe(1) site in the solution phase at room temperature. It is also shown that the trapped Xe is not released to solvent even after the CO is released from the Xe-trapped MbCO. We examined several possible dissociation schemes to explain the rate enhancement by blocking the Xe(1) site in detail and found that simple dead-end models could not account for the observed releasing rate. However, a branched path model with three intermediate states along the pathway can reproduce the essential feature well. According to this model, CO is trapped inside the Xe(1) site to retard the ligand escape from the protein. Although we cannot completely exclude a possibility that there are other models to reproduce the observed time profile of the TG signal, the results of the present experiment should be used as a criterion to judge the adequacy of other proposed models in future. The CO escaping time, the total volume change, and the volume change associated with the CO escape for the Xe-trapped MbCO are determined to be 400 ns, 2.9 $\pm$ 0.5 mL/mol, and 13 $\pm$ 1 mL/mol, respectively.

JA038877W